Controls of spatio-temporal patterns of soil respiration in a mixed forest

Julian Brzozon*[1], Patricia Schwarzkopf[1], Teja Kattenborn[2], Julian Frey[3], Friederike Lang[1], Helmer Schack-Kirchner[1]

[1]Chair of Soil Ecology, University of Freiburg, Bertoldstraße 17, 79098 Freiburg, Germany

[2]Chair of Sensor-based Geoinformatics, University of Freiburg, Tennenbacher Str. 4, 79106 Freiburg, Germany

[3]Chair of Forest Growth and Dendroecology, Tennenbacher Str. 4, 79106 Freiburg, Germany

*Corresponding author: julian.brzozon@soil.uni-freiburg.de

*ORCID: 0009-0001-5362-1842

Key-words: Tree distribution, vapour pressure, time-lag effects, hot spot, hot moments

Abstract

Introduction: Patterns of soil respiration (R_s) are heterogeneous on temporal and spatial scale. The most important controlling factors of soil respiration are microclimatic conditions such as soil temperature and moisture. However, a strong pronounced seasonality shifts R_s patterns from temperature to moisture-controlled regimes. Rarely investigated patterns are time-lagged effects prior to R_s measurements and influences of trees in mixed forests on large spatio-temporal scales.

Material and Methods: We investigated R_s over two years on a weekly to fortnightly measurement rhythm at an approximately 1 ha area in a mixed forest on 35 predefined locations using the common chamber technique. Analysis was derived using meteorological data and a tree species map.

Results: By tendency, R_s decreased with increasing distance to the tree and we observed significantly higher R_s in broadleaf patches compared to coniferous and mixed patches during the summer season (+27 %, +18 %, respective). Our data confirmed soil temperature and moisture as important controlling variables. Yet, our results highlight an additional predictor explaining a higher proportion in variability: the vapour pressure in the atmosphere. In contrast to soil temperature and moisture this predictor was able to track a collapse in R_s due to drought and increases following rewetting.

Conclusion: We conclude that meteorological conditions might be valuable indicators for CO_2 emissions from forest soils. Tree species distribution explained partly the spatial patterns and hot spots of R_s yet additional analysis of local soil properties will enhance our understanding of the soil plant interactions and the resulting R_s.

Abbreviations: CO_2 - carbon dioxide, R_s - soil respiration, T_s - soil temperature, Θ_S - soil moisture, VP_{cur} - current vapour pressure, VPD - vapour pressure deficit, H_{rel} - relative humidity, T_a - air temperature, DBH - diameter at breast height

Introduction

Soil respiration (R_s), the release of carbon dioxide (CO_2) from soils, represents the second largest terrestrial CO_2 flux and the biggest contributor to total ecosystem respiration (R_e) (Davidson et al. 2006; Goulden et al. 1996; Longdoz et al. 2000; Valentini et al. 2000). Even though temporal patterns showed similar trends, contrasting results of higher R_s compared to R_e were reported at various ecosystem scales (Barba et al. 2018). A certain proportion of this discrepancy may be explained by heterogeneity of R_s in ecosystems, as well as the existence and abundance of hotspots (Barba et al. 2018; Hereș et al. 2021; Scapucci et al. 2025). R_s is composed of heterotrophic respiration (R_{SH}) and autotrophic respiration (R_{SA}) (Kuzyakov 2006), while R_{SA} is seen as the main contributor to total R_s (Raich und Tufekciogul 2000). Thus, the big spatio-temporal variability of R_s may be controlled by the ecosystem structure (Köstler et al. 1968; Lejon et al. 2005; Søe und Buchmann 2005; Štursová et al. 2016).

Across forest ecosystems, only few studies have examined spatio-temporal patterns of R_s at broader scales (Darenova et al. 2024; Hereș et al. 2021; Ruehr und Buchmann 2010; Ruehr et al. 2010; Søe und Buchmann 2005). Among the known controlling variables, microclimatic conditions such as soil temperature (T_s) or soil moisture (Θ_S) are most commonly studied (Darenova et al. 2024; Epron et al. 1999; Hereș et al. 2021; Ruehr et al. 2010; Schindlbacher et al. 2012; Søe und Buchmann 2005; Subke et al. 2003; Wang et al. 2014a; Wang et al. 2014b). A widely accepted relationship between R_s and T_s can be described by site-specifically fitted exponential functions, which can often explain a high proportion of variability in R_s. From these functions, the increase in R_s by changes in T_s of 10 °C can be derived (Q_{10}). However, a simple use of this value neglects seasonality (Janssens und Pilegaard 2003) and important interaction effects with Θ_S (Lloyd und Taylor 1994; Qi et al. 2002). Even though R_s models based on T_s perform well (Lloyd und Taylor 1994; e.g. Ruehr et al. 2010), a rather minor (Ekblad et al. 2005) or indirect (Kuzyakov und Gavrichkova 2010) role of T_s was suggested due to time lag-effects. An increase in solar radiation during spring, peaking during the summer season (in temperate ecosystems), also drives changes in T_s (Kuzyakov und Gavrichkova 2010). Such meteorological conditions prior to R_s measurements represent rarely investigated control variables for R_s, but they might play a crucial role, as they drive ecosystem activity, highlighting the importance of plants as contributors to R_S in ecosystems due to the dependency of R_{SA} on photosynthesis (Davidson et al. 1998; Ekblad und Högberg 2001; Kuzyakov und Gavrichkova 2010; Moyano et al. 2008; Ruehr und Buchmann 2010; Tang et al. 2005b). Ekblad et al. (2005) and Bowling et al. (2002) highlighted the importance of lag-effects of the vapour pressure deficit (VPD) and are, to our knowledge, the only researchers using the VPD to explain patterns of isotopic signatures (^{13}C) of R_s, even though the VPD can be used as a proxy for ecosystem stress due to plant-specific stomatal behaviour as a response to VPD changes (e.g. Hsiao 1973; McAdam und Brodribb 2015; Sanginés de Cárcer et al. 2018). However, shorter-term lag effects of 2-4 hours were also determined for T_s, depending on soil depth (Ruehr et al. 2010).

Despite the fact that microclimatic conditions provide a good explanation for spatio-temporal patterns of R_s, the effect of forest structure is also of crucial importance observed by various studies. In a mixed forest with a high density of various tree species, Vesterdal et al. (2012) observed the highest R_s associated with European beech trees while in a mixed forest containing both pure patches and mixed patches, Khomik et al. (2006) observed the highest R_s associated with deciduous compared to coniferous patches, as well as a higher R_s associated with deciduous trees within the mixed patches. Similar to these results, Longdoz et al. (2000) reported higher R_s associated with European beech compared to Douglas fir patches within one forest. Jochheim et al. (2022) also report differences between deciduous and coniferous patches, but these varied between the measurement years depending on drought conditions. In an early literature review, Raich und Tufekciogul (2000) summarized in general 10 % lower R_s in coniferous forests in close proximity to deciduous forests. These contrasts in R_s associated with species composition may be due to tree specific habitats, as root systems (Köstler et al. 1968), as well as microbial and fungal community compositions (e.g. Hofmann et al. 2023; Prescott und Grayston 2013) and nutrient availability (e.g. Spielvogel et al. 2016; Vesterdal 1999; Vesterdal et al. 2013) depend on the tree species. Additionally, differences in photosynthetic activity between evergreen coniferous trees and the seasonal change in foliation of deciduous trees (Jochheim et al. 2022; Hansen et al. 1997; Curiel Yuste et al. 2004; Longdoz et al. 2000) are important drivers for spatio-temporal patterns of R_s. While tree species effects are common in the literature, only few studies highlight the distance to stemfoot effects on R_s as controlling variable (Jochheim et al. 2022; Scott-Denton 2003; Søe und Buchmann 2005), while Søe und Buchmann (2005) discovered no significant relationship between the distance to the closest tree and R_s rate in a European beech forest. However, Jochheim et al. (2022) observed constantly the highest R_s closest to the trees (1.25 m), compared to more distant positions (2.5 and 3.5 m), with more pronounced species-specific effects

during the summertime compared to the wintertime in pure stocks. In a higher elevated subalpine coniferous forest, Scott-Denton (2003) determined a negative correlation between the distance to the tree and the associated R_s, which was, however, more likely to be explained by the forest floor thickness. A further positive correlation regarding forest structural features was determined for the average diameter at breast height (DBH) of trees in proximity of up to 4 m to measurement position, which explained a considerable proportion in variability (Søe und Buchmann 2005). Due to these complex dependencies of R_s on spatio-temporal patterns, future trends of total R_S in the scope of climate change with extreme weather conditions such as heavy rain or extended drought periods (IPCC 2023) are uncertain because contributors to R_s as microorganism activity (Schindlbacher et al. 2011; Schindlbacher et al. 2012), root distribution (Brunn et al. 2022; Brunner et al. 2015) as well as spatially variable substrate availability, might alter with climate change (Brunn et al. 2022; Brunn et al. 2023). Dry periods can alter the pattern or R_s with collapse during drought and an increase in R_s due to rewetting, which was early discovered as the "birch-effect" (Birch 1958). However, this change in R_s was not evident in all cases, although there was a collapse and a re-establishment in R_s but not an extreme increase (Schindlbacher et al. 2011).

The goal of our study is to obtain reliable data for R_s from a mixed forest, to determine it's controlling factors and to quantify the contribution of predictor variables on R_s. We hypothesize that 1.) temporal patterns of R_s depends on T_s but an additional proportion in variation can be explained by meteorological parameters. 2.) R_s collapses during natural occurring drought and increases due to rewetting. 3.) due to species specific phenology R_s associated with deciduous trees is higher during the summertime, while R_s associated with coniferous trees is higher during the winter season and we also expect higher R_s closer to tree stems compared to R_s with a larger distance to tree stems, due to respiratory processes of trees. To test our stated hypothesises, we measured R_s on an area of around 10,000 m^2 at 35 predefined positions over 2 years and fitted it into a statistical model. This approach had also the aim to identify hot spots and hot moments in R_s. Following, we defined hot spots (Stutz und Lang 2023) as locations that, on average across the entire area (average of all measurement locations), reflect significantly higher R_s while cold spots are locations with significantly lower R_S than the seasonal averages. As hot moments, we defined phases in the temporal development of respiration that deviate from the pattern with unusual reactions (McClain et al. 2003), which we defined as changes in control variables (T_S). Our investigations are part of the collaborative research center ECOSENSE (Werner et al. 2024)with its joint research area called the ECOSENSE forest.

Material & Methods

Site description: The ECOSENSE Forest (Werner et al. 2024) is located in the south-western foothills of the Black Forest in Germany (48.2684336, 7.8779861, WGS84) with an average elevation of 465-475 m a.s.l.. Dominant tree species are European beech (*Fagus sylvatica* L.) and Douglas fir (*Pseudotsuga menziesii* Mirbel). Silver fir (*Abies alba*),

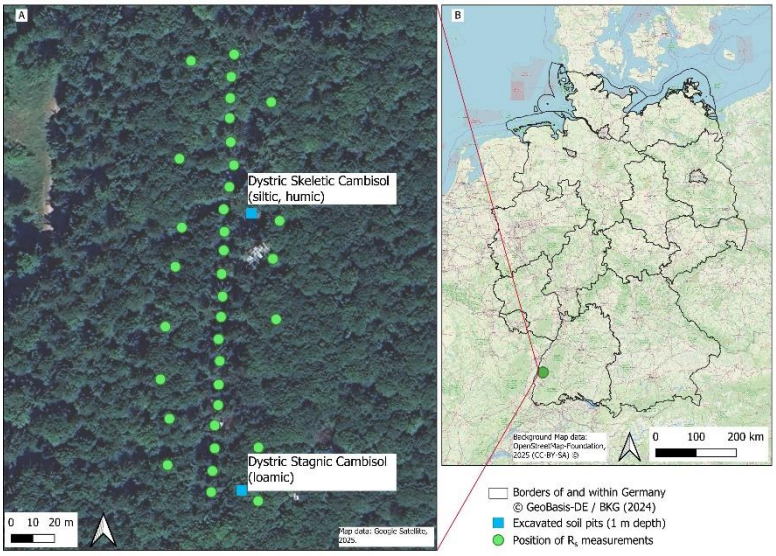

Figure 1: Location of the ECOSENSE Forest in Germany (B) and the setup of R_s measurement plots throughout the forest with location of soil profiles (A).

European larch (*Larix decidua* Mill.) and Norway spruce (*Picea abies* L.) also occur sporadically, and understorey vegetation is only sparsely developed. The entire stock is approximate 55-110 years old. The long-year (1981 – 2010) mean precipitation derived from the HYRAS dataset is 1000 mm yr^{-1}, with a mean annual temperature of 10°C (DWD 2025).

Soil Sampling: In November 2024, we excavated two soil profiles to a depth of 1 m to describe the existing soil types in the ECOSENSE Forest according to (IUSS 2022). We then sampled the soil to the defined horizons accodringly. Bulk samples were taken from the corresponding depth directly next to undisturbed rings (200 cm^3). Samples were then stored at 4°C until preparation for analysis.

The organic forest floor consisted of a patchy mull type with an averaging thickness of 2-4 cm. Two geological parent materials were present, resulting in two different soil types. In the southern part of the research area, we identified a Dystric Stagnic Cambisol (loamic) (IUSS 2022) derived from carbonate-free quaternary loess covering mesozoic sediments that are strongly weathered with redoximorphic features below a depth of 40 cm. In the northern part of the research area, we identified a Dystric Skeletic Cambisol (siltic, humic) (IUSS 2022) derived from carbonate-free quaternary loess, covering mesozoic sandstone with a high skeleton content. Below a depth of 40 cm only thin layers of fine earth between platy stones can be found.

Soil chemical analysis: Bulk samples were air dried (40°C) for at least 7 days and well mixed in between the days. After air drying, samples were sieved to 2 mm, with all visible roots, organic material and stones being sorted out. To determine the carbon to nitrogen ratio (C:N), soil was ground in a ball-mill (MM 400, Retsch GmbH, Germany), dried at 105°C and analysed using a CHNS elemental analyzer (vario EL cube, Elementar Analysensysteme GmbH, Germany). For cation exchange capacity (CEC), we followed the methods according to Trüby und Aldinger (1989) and analysed the extract with an ICP-OES (5800, Agilent, USA). For $P_{available}$, we used citric acid (1%) as extractant and followed standard methods (Gutachterausschuss Forstliche Analytik 2022). Analysis for $P_{available}$ was done with an ICP-OES (5800 ICP-OES, Agilent, USA). The pH-value was measured in H_2O following standard methods (Gutachterausschuss Forstliche Analytik 2022) using an automatic sampler (905 Titrando, Metrohm, Germany). Dissolved organic carbon (DOC) was extracted using a 1:2 water extract (König und Fortmann 1996) and measured using a total organic carbon analyzer (TOC-L, Shimadzu GmbH, Germany). Iron oxalate (Fe_{OX}) and iron dithionite (Fe_{DI}) were determined using the methods of Tamm (1922) modified by Schwertmann (1964) and measured on an ICP-OES (5800, Agilent, USA). Chemical soil properties of both profiles are presented in Table 1.

Table 1: Chemical soil properties of the two soil profiles in the ECOSENSE Forest. Values represent average values out of 3 laboratory analyses for the corresponding soil depth. Organic carbon content (C_{org}), carbon to nitrogen ratio (C:N), effective cation exchange capacity (CEC), base saturation (BS), dissolved organic carbon (DOC), available phosphorous ($P_{available}$), iron oxides as iron oxalate (Fe_{OX}) and iron dithionite (Fe_{DI})

Soil type	depth [cm]	pH_{H2O} [-]	C_{org} [mg g^{-1}]	C:N [-]	CEC [µmol_c g^{-1}]	BS [%$_{molC}$]	DOC [mg g^{-1}]	$P_{available}$ [mg g^{-1}]	Fe_{OX} [g kg^{-1}]	Fe_{DI} [g kg^{-1}]
Dystric Stagnic Cambisol (loamic)	0-7	4.8	21.6	11.8	74	3	0.4	26.4	4.2	16.2
	7-25	4.5	9.5	9.3	73	12	0.2	14.1	4.4	15.6
	25-38	4.6	3.6	5.1	96	5	0.1	3.9	3.3	16.3
	38-60	4.8	3.1	4.7	104	3	0.1	2.2	2.8	19.1
	60-80	4.8	1.5	2.4	100	3	0.0	0.5	1.4	17.2
	80-100	4.9	0.5	0.9	87	2	0.0	1.2	1.5	13.9
Dystric Skeletic Cambisol (siltic, humic)	0-7	4.3	25.7	14.5	75	5	0.4	43.2	3.6	9.3
	7-20	4.4	13.3	12.0	59	10	0.2	28.5	3.7	10.0
	20-42	4.4	11.0	12.0	56	14	0.2	21.4	3.7	10.3
	42-100	4.3	4.7	6.7	75	24	0.1	8.1	2.6	10.0

Soil physical analysis: Undisturbed ring samples (200 cm^3) were taken from the cooling storage and were placed in the laboratory with their lids closed untill the cylinders reached approximately room temperature. Cylinders were weighted and the gas diffusivity was subsequently measured using diffusivity chambers (900 cm^3). We used neon

(5 ml) as tracer gas, which was well mixed by fans in a chamber below the sample. After injection, we waited 15 minutes before performing the first gas analysis to ensure the tracer gas had diffused through the sample. Gas from the chamber was then drawn into a micro gas chromatograph (CP2002, Chrompack, The Netherlands) for six seconds. A total of six measurements were done for each sample with one flushing process before each measurement. The apparent diffusion coefficient (D_s) was then calculated by first Fick's law for gas flow. The relative diffusion coefficient (D_s/D_0) (Schack-Kirchner et al. 2001) was then calculated using the D_0 of Neon (0.297 $m^2 s^{-1}$) at 10°C. The samples were then saturated through a filter from the bottom side of the ring over the period of one week with a stepwise increase of water column. A water retention curve was created using the steps of -60 hPa, -300 hPa and -15000 hPa. After each drainage step, we also measured gas diffusivity. After -300 hPa we determined bulk density and porosity using a vacuum pycnometer. To determine -15000 hPa, we used a sub-sample with a height of 1 cm from the bottom part of the undisturbed ring sample. Afterwards the sub-sample and the sample were dried at 105°C to determine the residual water content. The fraction of the sub-sample at total dry weight was then used to calculate the -15000 hPa on the whole sample. To determine particle size, we took parts of the bulk samples after preparation for chemical analysis and analysed particles according to (Hartge und Horn 1989).

Table 2: Physical soil properties of the two soil profiles in the ECOSENSE Forest. Values represent mean values out of 3 laboratory analyses for the corresponding depth. D_sD_0 directly after field extraction (FF) and at water potential of -60 hPa and -300 hPa, porosity (ϕ_{soil}) and bulk density (ρ_{bulk}). Number of samples (n) corresponds to number of undisturbed rings available for these variables. Stones were estimated in field per horizon. Samples for particle size (n = 3 for each horizon) were taken from bulk samples. Due to high skeleton content below 42 cm in the Skeletic Cambisol, no undisturbed rings could be taken, therefore physical parameters were not determinable (n.d.). Standard deviations were ≤ 0.05 except for marked (*) values.

Soil type (IUSS 2022)	depth [cm]	*n*	D_s/D_0 FF [-]	D_s/D_0 -60 hPa [-]	D_s/D_0 -300 hPa [-]	ϕ_{soil} [-]	ρ_{bulk} [g cm^{-3}]	stones [$\%_{vol}$]	Particle size Clay [%]	Silt [%]	Sand [%]	Texture class
Dystric Stagnic Cambisol (loamic)	0-7	7	0.05	0.05	0.07	0.56	1.15*	0	34.4	58.5	7.0	Tu3
	7-25	8	0.05	0.04	0.05	0.53	1.24*	0	32.5	60.4	7.2	
	25-38	6	0.05	0.03	0.05	0.51	1.37*	3	39.2	53.5	7.3	
	38-60	10	0.03	0.01	0.05	0.45	1.54*	3	41.9	52.4	5.6	
	60-80	9	0.04	0.01	0.01	0.38	1.69*	8	43.5	52.5	4.0	
	80-100	9	0.01	0.01	0.01	0.35	1.79	3	34.8	58.2	7.0	
Dystric Skeletic Cambisol (siltic, humic)	0-7	7	0.06	0.04	0.06	0.57	1.07*	0	26.4	56.5	17.2	Lu
	7-20	7	0.07	0.04	0.07	0.54	1.22*	0	24.9	56.1	17.5	
	20-42	6	0.09	0.05	0.07	0.53	1.24*	17	26.5	54.3	19.2	
	42-100	-	n.d.	n.d.	n.d.	n.d.	n.d.	63	34.8	49.2	16.0	Lt2

Soil respiration measurements: R_s was measured manually over two years on an approximately weekly- to bi-weekly base (January 2023-December 2024). The 35 measuring plots as basic spatial investigation units (Figure 1) had an area of 2.25m^2. The open-bottom measuring chambers were randomly placed for the measurements without a permanently installed collar in the soil. For each measurement two open bottom chambers each equipped with a solid-state CO_2-probe (Vaisala GMP343, Vaisala Oyj, Helsinki, Finland) were placed directly on the forest floor. We did not use collars to prevent any disturbances to the soil, as collars were shown to potentially influence soil respiration measurements negatively depending on the insertion depth (Jovani-Sancho et al. 2017; Snell et al. 2014). During R_s-measurements, we also measured T_s in ca. 13 cm soil depth (GMH 3700 GES401, Seseca GmbH, Germany) and volumetric soil moisture (Θ_S) (SM150T, Delta-T Devices, UK) in ca. 5 cm depth. The plots for R_s measurements were established in December 2022 with distances of 10 m between each plot on a north-south transect (21 plots). Further plots were established (14 plots) east and west of the transect at a distance of approximately 20 m to the transect (Figure 1). To compensate for potential lateral leakage, we used a correction factor which was determined in the laboratory for measurements with the foam rubber (CF_F, Equation 1) and for measurements without any leakage prevention (CF_N, Equation 2). The measurement time was adapted to the expected flux (Fiedler et al. 2022): at the beginning of the measurement campaign, we started measurements with a length of 390 seconds (20

measurements, gap of 20 seconds). Initial analysis revealed that closing time could be reduced and was set to 190 seconds (20 measurements, gap of 10 seconds). Since the measurement time was shortened, we were able to measure all plots within one day (since June 2023). Prior to this change, the plots were selected randomly and not every plot was measured within one day. On three days, measurements were not completed due to weather conditions or system error (once only 33/35 plots and twice only 26/35 plots). Both individual measurements have been averaged to a plot mean per measuring day. Due to technical problems in 89 of 2295 (4%) cases, R_s was measured only with one chamber. The order of measuring plots was set randomly for each day in order to prevent any bias due to diurnal patterns (Ruehr et al. 2010). For R_s flux calculation 50 seconds were cut off at the beginning and at the end of each single measurement due to saturation effects at the end or slow increase at the beginning. In very few cases we needed to adapt the time manually, as the device stopped the recording (< 1 %).

$$CF_F = 1.49 + 0.007 * (\frac{T_a+T_s}{2}) \quad (1)$$

$$CF_N = 1.96 + 0.013 * (\frac{T_a+T_s}{2}) \quad (2)$$

With T_a = air temperature in °C and T_s = soil temperature in °C.

Forest stock features: A forest inventory was conducted in the core area of the ECOSENSE forest (circa 3 ha; Werner et al. 2024). All trees with a diameter at breast height (DBH) ≥ 7 cm were recorded in the field, including species identity, DBH, and spatial position. Tree locations were initially determined using an EMLID RTK GNSS system (EMLID REACH RS2, Emlid Tech Kft. Budapest, Hungary). Subsequently, terrestrial laser scanning (TLS) was carried out using a Riegl VZ-400i (RIEGL Laser Measurement Systems GmbH, Horn, Austria) along multiple transects to capture the stand structure in high detail. The resulting point clouds were used to refine (optimize) the geolocation of individual tree positions and to derive tree heights for the complete inventory.

Comparable to Søe und Buchmann (2005) we calculated the distance to the nearest neighbouring tree. Additionally, we buffered a zone around the measurement position (5 m radius) and calculated the average distance to all trees, the number of trees and the average DBH within the buffered area. We used the distance of 5 m to include all plots into analysis, as the maximum nearest neighbouring distance was 4.5 m. Since not only *Fagus sylvatica* and *Pseudotsuga menziesii* were within the buffer zone we grouped the tree species according to the species composition, which are also referred to as these groups in the following: deciduous (pure *Fagus sylvatica* composition [18 plots]), coniferous (either pure *Pseudotsuga menziesii*, [8 plots] pure *Abies alba* [1 plot] or *Pseudotsuga menziesii* mixed with *Abies alba* [2 plots]) and mixed (always containing *Fagus sylvatica* mixed with different contributions of *Pseudotsuga menziesii, Abies alba, Larix dedidua, Picea abies* [6 plots]). The number of trees within the buffer zone of 5 m varied between 1-10 trees.

Meteorological data: At the beginning of the measurement period no reliable weather data were available from the ECOSENSE weather monitoring, so we decided to use the HYRAS dataset (DWD 2025) which represents modelled data of daily precipitation (Rauthe et al. 2013), minimum, maximum and average air temperature (T_a), relative humidity (H_{rel}) (Frick et al. 2014; Razafimaharo et al. 2020) for the specified cell covering the ECOSENSE Forest (5x5 km cell-size). We calculated the saturated vapour pressure (VP_{sat}) using Teten's equation with corrections for positive and negative average T_a, which was then converted to actual vapour pressure (VP_{act}) by multiplication with H_{rel}. The vapour pressure deficit (VPD) was calculated by subtraction of VP_{act} from VP_{sat}. Wind velocity and global radiation data were extracted from ERA5-Land datasets (Copernicus Climate Change Service (C3S) 2019; Muñoz-Sabater et al. 2021), which also represents a modelled grid covering the ECOSENSE Forest (11 x 7 km cell size). As a smooth model parameter of seasonality we calculated the negative cosine of the Julian day of the year (cos_{doy}), (e.g. Sims 1974) with positive, increasing values during the mid of the year (+1) and decreasing, negative values during the start and end of the year (till -1). We also calculated the negative sine of the Julian day of the year (sin_{doy}), which then creates the same effect but shifted by three months, and therefore represents the spring and autumn season. This method takes into account a transition with a development, apart from standard seasonal classification, which cumulates three months to only one variable and is therefore specifically well suited for model predictions. In order to obtain more general statements about the seasonal effects in addition to the cos_{doy} we also used the classical seasonal classification according to the German weather service (DWD) and averaged the values over the seasons for a more common evaluation. Seasons were classified as Winter: December – February, Spring: March – May, Summer: June – August, Autumn: September – November.

Statistical analysis: To determine the predictors for **temporal patterns** in R_s we used linear models (lm from stats-package, R Core Team 2023) applied to the average R_S values from the measuring days of all 35 sampling plots. As predictors, we used the respective average weather parameters from the day of the measurements of R_s as well as aggregated mean or summarised values of these predictors 1-7 days prior to the measurement day. To prevent model overfitting and to identify predictors that provide meaningful information on the development of R_s only predictors with an R^2 above 0.4 were taken into consideration for the further model optimization. We also tested the model for normal distribution and heteroscedasticity using analytical plots. If the common problem of heteroscedasticity was present, we calculated robust standard errors using HC4 (Hayes und Cai 2007). Additionally, we also applied different methods to determine temporal patterns by checking dependencies of R_s on T_s alone (equation 3) and in combination with soil moisture Θ_S (equation 4). We also calculated Q_{10} values (equation 5) using non least square models (nls from stats-package, R Core Team 2023) with fitted parameters.

$$R_s = a * e^{b*T_s} \tag{3}$$
$$R_s = c * \Theta_s * e^{d*T_s} \tag{4}$$
$$Q_{10} = e^{10*b} \tag{5}$$

With R_s = the modelled soil respiration [µmol CO_2 m^{-2} s^{-1}], T_s = soil temperature [°C] at reference depth (13 cm) and Θ_s [‰vol]. a, b, c, d were fitted using non least square models.

To visualize and determine **spatial patterns,** we used inverse distance weighting (idw from phylin-package, Pebesma 2018; Pebesma und Bivand 2023; Tarroso et al. 2015; Tarroso et al. 2019). Dependencies of R_s on forest structural features were tested using linear models (lm from from stats-package, R Core Team 2023) and pairwise wilcox rank sum tests (from stats-package, R Core Team 2023) for group comparisons. Answering the question whether (seasonal) **hot spots** for R_s exist in the ECOSENSE Forest, we calculated a mixed effects model (lmer from lme4, Bates et al. 2015) with the measurement plot as explanatory variable, but the day of the measurement as a random effect. From this, we calculated estimated marginal mean values (emmeans from emmeans package, Lenth 2023) and set those in contrast (contrast from stats-package, R Core Team 2023) to the averaged values of the corresponding season, to identify plots with statistically significant higher or lower deviations from the averaged seasonal R_s. To identify **hot moments**, we used linear models (lm from stats-package, R Core Team 2023) and spearman correlation (cor from stats-package, R Core Team 2023) tests to check for unusual patterns between R_s and T_s. All statistical analysis was done in RStudio 2023.06.0 based on R4.2.3 (R Core Team 2023). For data organization we used the tidverse (Wickham et al. 2019), ggplot2 (Wickham 2016) and lubridate packages (Grolemund und Wickham 2011).

Results

Weekly to fortnightly soil respiration measurements

In total, 4507 single R_s measurements were available for data evaluation, which were merged to 2295 measurements on the plot level on a total of 72 measurement days. Annually averaged R_s in 2024 (3.10 ± 1.86 CO_2 µmol m^{-2} s^{-1}) was higher than in 2023 (2.74 ± 1.89 CO_2 µmol m^{-2} s^{-1}). The highest daily averaged R_s was reached in 2023 (7.74 ± 2.0 µmol CO_2 m^{-2} s^{-1}), while the highest daily averaged R_s was lower by almost 1 µmol CO_2 m^{-2} s^{-1} in 2024 (6.83 ± 2.44 µmol CO_2 m^{-2} s^{-1}). On plot level, the highest R_s was reached in 2023 with 27.1 µmol CO_2 m^{-2} s^{-1} which was lower by 11.4 µmol CO_2 m^{-2} s^{-1} in 2024 (data not shown). We identified strong seasonal fluctuations with peak R_s during summertime with only small differences between the two years, but high differences between the seasons within one year (Table 3). Unfortunately, the measurement device for Θ_S broke down in January 2024 due to high skeleton content in one plot and measurements were not possible thereafter. The two years differed in the precipitation amount: in 2023 annual precipitation was 37 mm below the long year average, in 2024 it was 106 mm above. The VP_{cur} was similar for both years but showed deviations during the summertime with an averaging higher VP_{cur} during summer 2023, while the VPD also deviated by averaging 0.19 kPa during both summer seasons (Table 3). In both years, the VP_{cur} and VPD showed seasonal variation as well and followed the development of R_s. Also, the determined Q_{10} values (Equation 5), using the daily average R_s and T_s, revealed seasonal variability with the highest Q_{10} for both winter season in both years. However, the highest Q_{10} during winter 2023 exceeded the Q_{10} in winter 2024 by a factor of 2.6. In 2023 the Q_{10} continuously decreased till autumn, whereas in 2024, the lowest Q_{10} was reached in the summer season. Calculating the Q_{10} based on values throughout the whole year, the Q_{10} for both years were similar

with 3.32 ± 1.22 and 3.11 ± 1.12 in 2023 and 2024, respectively. The correlation matrix separated by season (Table 4) revealed the different responses of R_s in relation to the climate predictors. Interestingly, the daily average R_S correlated differently with the presented meteorological parameters across seasons, showing the lowest correlations and even negative correlations in some cases during the summer for all parameters except for Θ_S in 2023, although positive correlations were observed during the other seasons.

Table 3: Seasonal averaged soil respiration (R_s), with number of measurement days (n) within the respective season, mean soil temperature (T_s) during R_s measurement campaigns and soil moisture (Θ_S). All values are averaged per season for the corresponding years of measurement on the ECOSENSE Forest and given with standard deviation. Q_{10} values were calculated for each season and years separately and given with standard errors from the fitted model. From the HYRAS dataset we summarised precipitation (∑ Prec.) and averaged air temperature (T_a), current vapour pressure (VP_{cur}) and vapour pressure deficit (VPD).

Year	Season	**R_s** [µmol CO_2 m^{-2} s^{-1}]	n	T_S [°C]	Q_{10}	Θ_S [‰vol]	∑ Prec. [mm]	T_a [°C]	VP_{cur} [kPa]	VPD [kPa]
2023	Winter	**1.07 ± 0.53**	8	4.8 ± 1.4	20.4 ± 2.1	33.0 ± 3.5	174.2	3.9 ± 3.9	0.67 ± 0.18	0.16 ± 0.09
	Spring	**1.98 ± 1.12**	10	8.7 ± 2.8	2.9 ± 1.9	33.2 ± 3.8	234.1	9.6 ± 4.5	0.92 ± 0.27	0.33 ± 0.2
	Summer	**4.83 ± 2.07**	10	15.8 ± 1.7	2.8 ± 2.1	16.3 ± 4.5	279.6	19.4 ± 3.1	1.53 ± 0.33	0.75 ± 0.34
	Autumn	**2.76 ± 0.96**	10	13.4 ± 3.1	2.1 ± 1.4	17.7 ± 9.9	275.1	12.1 ± 5.8	1.16 ± 0.36	0.35 ± 0.24
2024	Winter	**1.14 ± 0.44**	7	5.1 ± 1.3	7.9 ± 2.9	n.d.	181.4	3.7 ± 4.3	0.68 ± 0.19	0.15 ± 0.09
	Spring	**2.30 ± 1.09**	10	8.9 ± 2.1	5.1 ± 1.5	n.d.	374.3	10.5 ± 4.3	0.98 ± 0.23	0.33 ± 0.22
	Summer	**5.36 ± 0.93**	9	16.1 ± 2.1	1.4 ± 1.4	n.d.	282.3	19.0 ± 3.0	1.67 ± 0.28	0.56 ± 0.23
	Autumn	**3.27 ± 1.49**	8	12.6 ± 3.2	3.5 ± 1.2	n.d.	267.9	10.5 ± 4.9	1.13 ± 0.35	0.20 ± 0.13

Table 4: Correlation matrix (Spearman-correlation coefficients) between average R_s and potential meteorological predictors (current daily values compared to daily averaged R_s) and the seven day (7-d.) aggregated values prior to the measurement day separated by season for the two measurement years. Climate predictors are the vapour pressure deficit (VPD), current vapour pressure (VP_{cur}), air temperature (T_a), global radiation (Glob-Rad), daily soil temperature (T_s) and soil water content (Θ_S).

Year	Season	VPD		VP_{cur}		T_a		Glob-Rad		Prec		T_s	Θ_S
		daily	7-d.	daily	7-d.	daily	7-d.	daily	7-d.	daily	7-d.	daily	daily
2023	Winter	0.17	-0.36	0.76	0.62	0.69	0.57	-0.07	-0.29	0.30	0.26	0.88	0.05
	Spring	0.2	0.26	0.78	0.77	0.65	0.59	0.53	0.46	0.29	0.05	0.64	0.6
	Summer	-0.6	-0.32	0.48	0.55	0.03	0.14	-0.39	-0.55	-0.33	0.65	0.53	0.6
	Autumn	0.22	0.37	0.79	0.78	0.38	0.67	0.49	0.58	-0.07	-0.04	0.64	-0.3
2024	Winter	0.71	0.64	0.68	0.89	0.68	0.82	0.21	0.39	0	0.57	0.64	-
	Spring	0.42	0.58	0.83	0.96	0.73	0.9	0.2	0.54	0.66	0.08	0.95	-
	Summer	-0.25	-0.22	0.17	0.33	0.22	0.16	0.07	-0.1	0	0.65	0.42	-
	Autumn	0.14	0.33	0.68	0.81	0.43	0.81	0.38	0.48	-0.07	-0.29	0.48	-

Hot moments of R_s

During the transition between spring and summer in 2023 average R_s collapsed from 10th May until 16th June by 3 µmol CO_2 m^{-2} s^{-1}. This phase was characterised by increasing T_s and T_a but low precipitation and no precipitation on 29/38 days (Figure 2). After the last higher rain event on 21st May (14.5 mm d^{-1}), the weather remained dry and only a low rainfall event on 4th June with 1.4 mm d^{-1} (0.14 % of 30-year average) occurred, causing a slight increase in R_s (7th June) by 0.72 µmol CO_2 m^{-2} s^{-1}, but a further decrease in the following week. During this whole phase, Θ_S dropped on average by 24 ‰vol. With an onset of rainfall from 18th June till 22nd June with a total of 29.5 mm (approx. 3 % of 30-year average) out of which 20 mm d^{-1} fell within just in one day (13th highest rainfall event over the two years) a sharp increase in R_s by 6.26 µmol CO_2 m^{-2} s^{-1} was measured on 23rd June, while average T_s and Θ_S increased only slightly by 1.5 °C and 1.3 ‰vol, respective. The day after the strong rainfall event represented the highest R_s (7.74 ± 2.0 µmol CO_2 m^{-2} s^{-1}) in the measurement period. Additionally, VPD increased from 22nd May until 12th June by 0.94 kPa but decreased directly afterwards till 23rd June by 0.33 kPa following the larger precipitation events (Figure 2). During this phase the maximum average VPD was 1.37 kPa. The correlations between R_s and T_s as well as VPD, were negative during this phase (ρ_s = -0.77 and ρ_s = -0.94, respective), but positive between R_s and Θ_S (ρ_s = 0.83). After the stronger rainfall event R_s dropped after the maximum efflux by averaging 4.4 µmol CO_2 m^{-2} s^{-1} just six days later. The second highest R_s (7.3 ± 4.1 µmol CO_2 m^{-2} s^{-1}) over the two years was reached two months later in August. In general, total R_s was higher during 2024, but the two highest rates in R_s were reached in 2023 and exceed those

from 2024 by 0.5 – 1.2 µmol CO_2 m^{-2} s^{-1}. However, we also identified additional phases characterized by low precipitation and low Θ_S i.e. during the end of August 2023 which was not as prolonged as the aforementioned phase. In comparison to VPD, we identified around 10 additional but shorter time periods in which VPD and R_s were

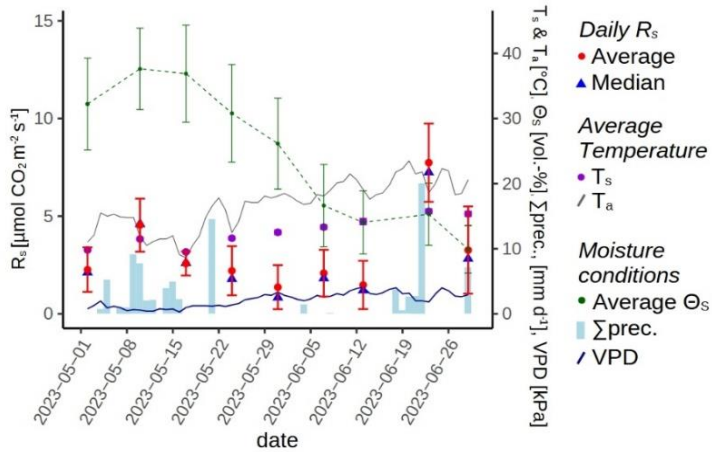

Figure 2: Extract of the timeseries from May – June 2023 for mean and median for soil respiration (R_s), mean soil temperature (T_s), mean soil water content (Θ_S), daily summed precipitation (∑prec.), mean daily air temperature (T_a) and mean daily vapour pressure deficit (VPD).

correlated negatively.

Regression models with meteorological and microclimatic parameters

To explain the temporal variability, we compared three models using linear and exponential fits. All models based on the daily average of R_S from all 35 plots and the abiotic predictors (Table 5). All correlation coefficients between the predictors are listed in the supplemental materials (Figure S1).

Table 5: Explanation of variability (R^2) of averaged daily R_s for climate variables as predictors with p-value determined with linear models and spearman correlation coefficients (ρ_s) between R_s and climate variables over the two measurement years. Θ_S only for the year 2023. Note: values were round to two decimal digits.*

Predictor	R^2	p-value	ρ_s	Aggregated predictors	R^2	p-value	ρ_s
VP_{cur}	0.73	***	0.88	7-day mean	0.78	***	0.91
T_s	0.68	***	0.86	-	-	-	-
T_a	0.57	***	0.79	7-day mean	0.64	***	0.83
cos_{doy}	0.50	***	0.73	-	-	-	-
Global radiation	0.31	***	0.61	7-day sum	0.32	***	0.62
Θ_S*	0.20	*	-0.48	-	-	-	-
VPD	0.17	***	0.59	7-day mean	0.30	***	0.66
sin_{doy}	0.16	***	0.42	-	-	-	-
Wind-velocity	0.08	***	-0.25	7-day sum	0.22	***	-0.54
H_{rel}	0.01	/	-0.31	7-day mean	0.03	/	-0.25
Precipitation	-0.01	/	0.16	7-day sum	0.02	/	0.19

In the following we present three models:

1. *Meteorological model*: The highest contribution to explain the variation of R_s is represented by the 7-day-mean VP_{cur} (Table 5). We did not include T_s into our model due to high co-linearity with the VP_{cur} and the 7-day mean VP_{cur} which created variance inflation factor (VIF) > 3. T_a is already combined in the VP_{cur} and does not need to be included as a separate predictor. As the next highest predictor, we included the cos_{doy} which

resulted in VIF-values of < 3 (R^2 = 0.78). However, residuals of this model contained high information content and were systematically explainable in all seasons by positive relationship with VPD (Supplemental material Figure S3). We therefore needed to introduce a new predictor, which were the residuals the model, explaining the variation of VPD by using the VP_{cur} (R^2 = 0.75). The residuals of this model represent low, wet VPD as negative value and high, dry VPD as positive value and represents therefore the humidity of the atmosphere. We could not include the original VPD due to high co-linearity between VP_{cur} and VPD. Including the new predictor increased explanation in variability by 6 % (R^2 = 0.84) with VIF-values < 3.

2. *Exponential T_s model*: The exponential model fit using T_s as a predictor (Equation 3) described a similar proportion in variability (R^2 = 0.68) as the linear fitted model (Table 5). However, comparisons on aggregated values prior to the measurement day were not possible as T_s was only captured during R_s-measurement.
3. *Exponential T_s and Θ_S model*: This model could only be used for the 2023 due to missing Θ_S in 2024. For comparison, the prescribed models were also fitted only for 2023. The exponential fit of T_s and Θ_S (Equation 4) resulted in a lower explanation in variability (R^2 = 0.72) than the model using the exponential fit of T_s alone (Equation 3, R^2 = 0.78). A similar explanation in variability was represented by the *meteorological model* (R^2 = 0.77). If we compare the models only for 2024, the exponential fit of T_s delivered the highest explanation in variability (R^2 = 0.82). However, if we separate the models by years, the 7-day mean VP_{cur} still delivers the highest explanation in variance in 2024 (R^2 = 0.89) but lower explanation in variance in 2023 (R^2 = 0.69).

Application of the *meteorological model*

For further analyses we focused on the best model, the meteorological (Equation 6) model explaining 87% of the total variability. This model left lower residuals compared to both other models using T_s and Θ_s as predictors especially during "hot moments" such as dry and hot weeks in 2023 (Supplemental Material Figure S4). The model followed generally the measured values well, but smoothes to a certain degree the data. The boxplots of the model residuals (Figure 3, B) contained a seasonal pattern with a systematic overestimation in spring and autumn and an underestimation in summer. These seasonal effects could obviously not be covered by the seasonal term (cos_{doy}) in the model. Due to heteroscedasticity, we calculated robust standard errors (Supplemental Material, Table S1).

$$R_s = -0.69 + (3.24 * 7d.VP_{cur}) + \left(0.7 * cos_{doy}\right) + (-2.11 * res_{VPD}) \quad (6)$$

With R_s in µmol CO_2 m^{-2} s^{-1}, 7d. VP_{cur} as 7-day mean VP_{cur}, cos_{doy} as cosine of the day of the year and res_{VPD} as residuals from model explaining the VPD using VP_{cur}.

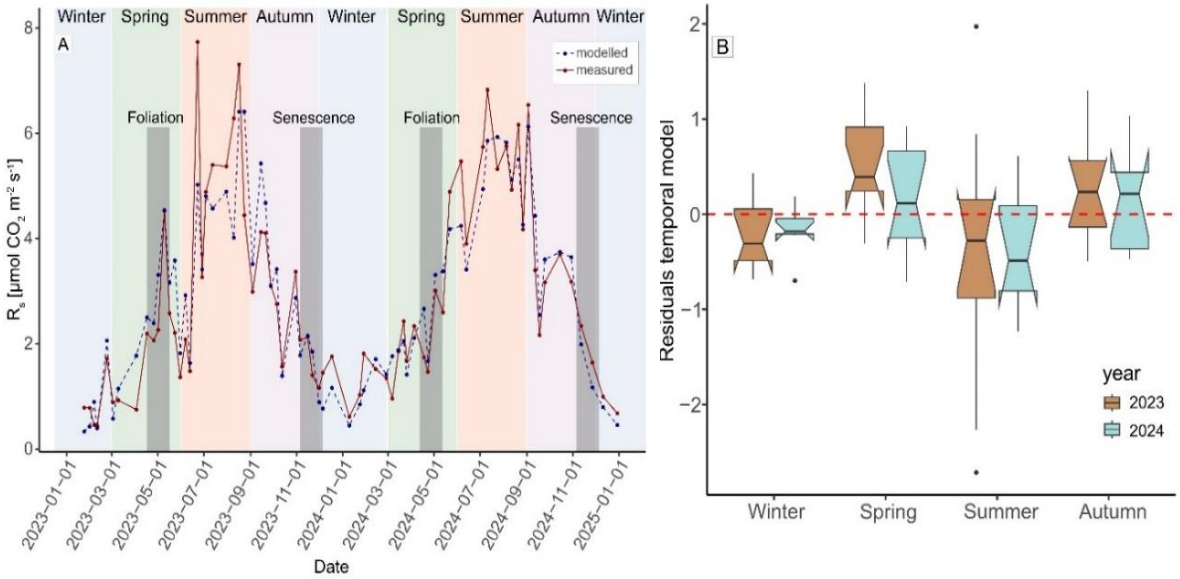

Figure 3: Temporal model (A) for R_s [µmol CO_2 m^{-2} s^{-1}] for both measurement years in comparison to measured R_s (daily averaged) and residuals of the model (B) separated by year.

Spatial predictors – hot spots of R_s and the influence of forest structure

The comparison of plots at the individual plot level, separated by season, presented the development over the two years per season (Figure 4, A) and illustrated a spatial pattern of R_s within the ECOSENSE Forest. Analysing the hot and cold spots (significantly higher or lower R_s) separated by season and tree species composition revealed particularly one plot, which was always considered a hot spot, whereas all other hot and cold spots occur only in specific seasons (Figure 4, A). The patterns stayed almost persistent throughout both measurement years. The largest occurrence in hot spots was determined for the summer season within deciduous species composition. The plot-wise

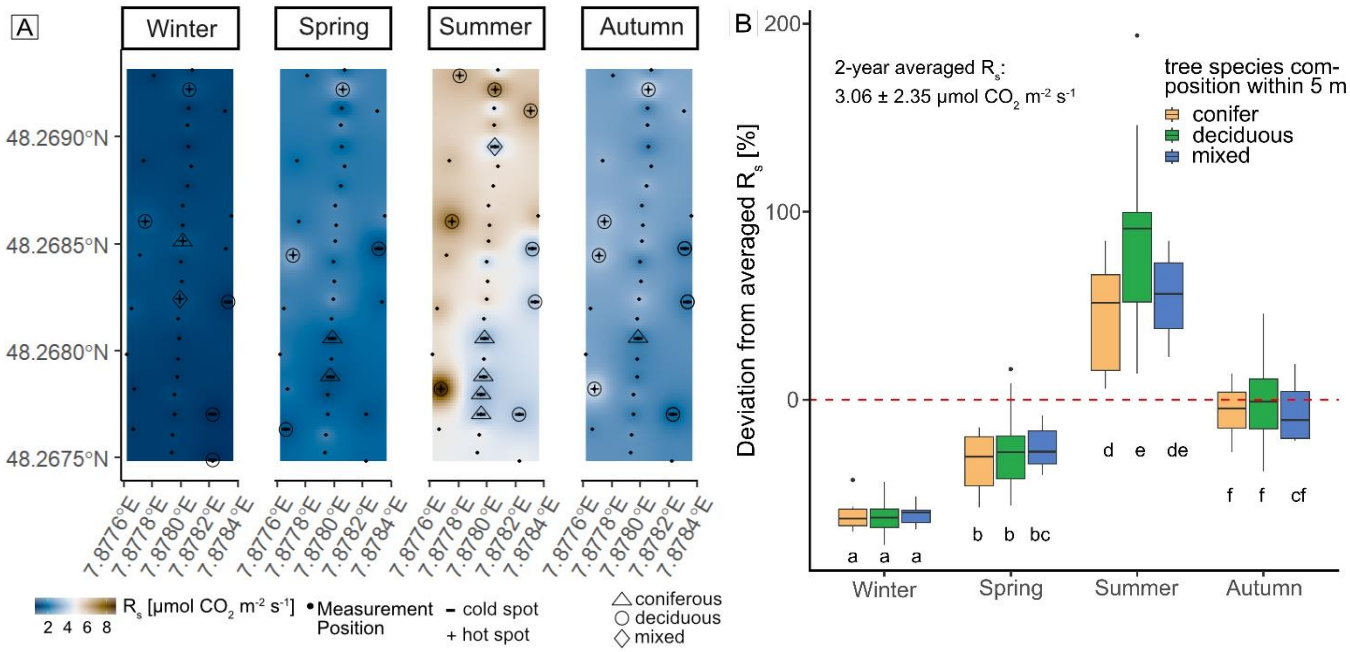

Figure 4: Spatial variability of soil respiration (R_s) over two measurement years (2023 - 2024) plotted on a part of the ECOSENSE-Forest area using inverse-distance-weighting separated by season (A) and distribution of average deviation from mean R_s separated by season and tree species composition (B).

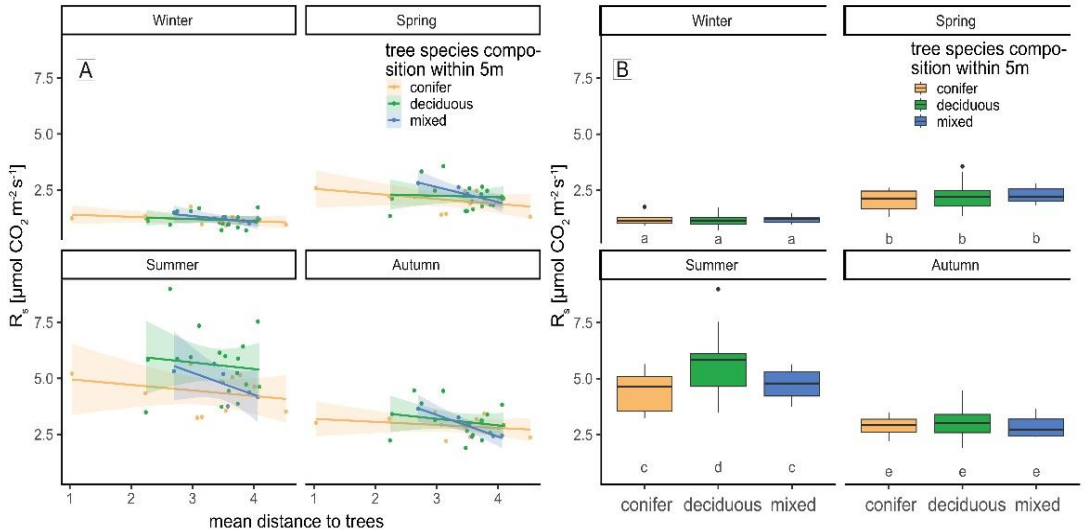

Figure 5: Soil respiration (R_s) in dependence to distance to trees (A) and in dependence of tree species composition and season (B).

deviation from the averaged R_s (over the whole measurement period) separated by species composition and season (Figure 4, B) was significantly different between every season except for the comparison between mixed composition during spring and autumn. In contrast, within a season, deviations from the average R_s separated by species composition were only significantly different within the summer season. In general, the deviation from the overall average R_s was less pronounced during the autumn season, with the slightest average deviation for deciduous composition (Figure 4, B)

Due to the strong seasonal patterns (Table 4, Figure 4), we averaged R_s per plot per season and analysed the dependence of R_s on stand structural features of the surrounding area. The R_s associated with tree compositions was significantly different between every season (Figure 5, B). Within the single seasons, only during summertime, the R_s associated with deciduous trees were significantly different from the other two species compositions. We detected a slight negative relation between average distance to trees within the buffer zone and R_s, as well as with the nearest neighbouring tree, which was more pronounced during the vegetative seasons (spring, summer, autumn), but not significant (Figure 5, A). A comparison to the average DBH of surrounding trees within the 5 m buffer zone showed a positive relationship between R_s rate and deciduous and mixed composition during summertime, whereas the relationship between R_s rate and DBH was negative for coniferous composition. In comparison to tree height, we determined a negative relationship of tree height for deciduous and coniferous species during the vegetative season, whereas mixed composition showed a positive relationship. Explaining the variability in R_s as average per year with average distance to trees or nearest neighbouring distance was only significant, if seasonality was included as predictor, whereas seasonality explained the main part of the variability in R_s. The same pattern was determined for the DBH and tree height as predictors (data not shown).

Discussion

Temporal patterns in R_s are determined by meteorological conditions prior to measurements

Both, the observed rates of R_S and its seasonality are typical for European forest ecosystems (Hereș et al. 2021; Ekblad et al. 2005; Jochheim et al. 2022; Ruehr und Buchmann 2010; e.g. Ruehr et al. 2010; Scapucci et al. 2025; Søe und Buchmann 2005; Subke et al. 2003). We hypothesised that R_s depends on soil temperature T_s but also on meteorological conditions, in parts with a time lag to the actual measurement. A comparison of the three models presented (*meteorological, exponential Ts, exponential Ts and soil moisture Θ_S),* clearly revealed that the *meteorological model* we proposed performed best. The strong, linear relationship between R_s and the (averaged) atmosheric vapour pressure VP_{cur} stands out and has not been described so far. VP_{cur} combined exponential air temperature T_a and relative humidity H_{rel} in one variable. The positive relationship indicated the importance of available atmospheric water for temporal R_s patterns. However, a very high correlation between the VP_{cur} and T_s and a high co-linearity between T_s and the VP_{cur} was present which could be a reason why we were able to replace the usually used T_s by the VP_{cur} in our model. T_s might reflect a better predictor for R_s estimation in other research, as reference depths were different. We measured T_s in 13 cm depth, while e.g. Moyano et al. (2008) found highest correlation with T_s in 2 cm depth. Another study suggested T_s measurements within 1-5 cm depth for lag estimations, but presented for depths of 10 cm an exceptionally high Q_{10} (Ruehr et al. 2010) which can not be supported by our findings of Q_{10} values. The values determined in our study were similar to the Q_{10} determined by Khomik et al. (2006) from 2 cm soil depth. We also calculated seasonally separated Q_{10} values as suggested by Khomik et al. (2006) with the limitation that a temperature range of up to 10 K within one season are unrealistic. The higher Q_{10} values during wintertime and lower Q_{10} during summertime suggest a shift from a temperature-controlled to a climate/moisture-controlled regime in summer. Additionally, the change in correlations between R_s and Θ_S and the summarized precipitation (Table 4) underlined our assumption, as correlation was higher during the spring and summer season, while reversed for the other predictors. A similar change in controls in R_s was also suggested by Hereș et al. (2021).

As T_s was only measured in combination with R_s, we cannot make any more precise statements about lag-effects of T_s on R_s, as e.g. Ruehr et al. (2010). However, we also point out to a strong correlation between T_s and global radiation and the summarised global radiation and linear relationship in T_s and therefore highlight the effect of global radiation on T_s development (Kuzyakov und Gavrichkova 2010). For long-term available predictors in every case, the aggregated values prior to measurements correlated highest with R_s and we thereby support the assumptions that

lag-effects are crucial for R_s patterns on temporal scale (Bowling et al. 2002; Ekblad et al. 2005; Kuzyakov und Gavrichkova 2010).

Even though the *meteorological model* performed well, the residuals showed a larger range during the vegetation season. These differences could be driven by the activity of the ecosystem. During wintertime, the ecosystem stays dormant due to lower temperatures, short daylight and the absence of foliage of deciduous trees and absolute R_s is low. Photosynthetic activity is at rest except for coniferous evergreen trees (Hansen et al. 1997; Jochheim et al. 2022) and due to lower T_s and low nutrient availability, microbial activity as well. Photosynthetic activity with its peak during the summer drives R_{SA} and therefore the total R_s (Kuzyakov und Gavrichkova 2010; Tang et al. 2005b). Microbial activity is also higher during the summer season, because enzymatic activity depends on T_S (Carey et al. 2016; Schindlbacher et al. 2011; Schindlbacher et al. 2012) but also on root exudate availability, which in turn is driven by photosynthesis (Kuzyakov und Gavrichkova 2010). The inverse or lower correlations with most of the presented meteorological predictors (Table 4) further underline the importance of the phenology on temporal R_s patterns. Yet for this research solar radiation is the only available predictor as a proxy for photosynthetic activity, besides the manual observation of leaf developmental stage. The latter resulted in a direct increase in R_s due to foliation and decrease in R_s due to senescence (Figure 3, A). Therefore, we implemented smooth seasonal shifts with the cosine angle function cos_{doy} in our model, which created a peak during summertime. This still lacks the true representation of the phenology. The overestimation during spring could be due to the fact that trees invest sugars into biomass at first (Kuzyakov und Gavrichkova 2010) and therefore R_s does not follow the steady increase of the VP_{cur}. Furthermore, R_{SH} might be low, due to low exudation of easily available substrates in the rhizosphere. However, our model created during summer 2023 a broader range in residuals which can simply be attributed to the dry phase (hot moment). During this dry period the model is not capable in representing the high variability in responses to the rainfall event after the dry phase. This suggests a strong spatial and individual response on plot-level. The widely applied models using T_s as the only predictor or in combination with Θ_S, especially during extreme events in R_s, did not deliver the same performance as our presented model (Supplemental Material Figure S4). For models using T_s as predictor it was already shown, that available Θ_S is a limiting factor (Ruehr et al. 2010).

Collapse of R_s and increase due to rewetting

In our second hypothesis we stated that R_s will strongly decrease during drought periods and increases after rewetting. We were able to clearly identify one rewetting period as an actual "hot moment" of R_S. The usual pattern of positive correlation between T_s and R_s was reversed due to a decline in Θ_S caused by a precipitation deficit. Rewetting led to an extreme increase in R_s. This increase was also reported in the literature (Birch 1958; Jochheim et al. 2022; Ruehr et al. 2010; Tang et al. 2005a). However, this effect has not always been confirmed. Schindlbacher et al. (2012) observed a decline due to drought and a regeneration of R_s due to rewetting, but not a peak. The authors attributed the lack of this effect to the importance in homogeneous rewetting of the forest floor, which might not have occurred due to preferential flow paths created by drought induced hydrophobicity (Schindlbacher et al. 2012). Overall, the data obtained confirm our hypothesis and we suggest, that the strong increase was an effect of reactivation of microbial activity (R_{SH}) (Birch 1958; Jochheim et al. 2022; Ruehr et al. 2010; Wang et al. 2014a; Wang et al. 2014b). Jochheim et al. (2022) additionally suggested a potential collapse in R_{SA} associated with *Fagus sylvatica* due to a stronger decline associated with these species, which cannot be supported by our data, as all plots were affected similarly. However, we cannot exclude that R_{SA} was not affected by the drought period. The vapour pressure deficit VPD can also be used as an estimate for aboveground plant stress, as trees open or close their stomata when VPD is low or high, respectively (McAdam und Brodribb 2015). In comparison, the summer and autumn of 2023 showed a higher VPD than 2024, indicating drier aboveground conditions, especially during the rewetting peak. The strongly differing correlations of VPD and R_s in the individual seasons underline the VPD as an important factor for R_s patterns. Sanginés de Cárcer et al. (2018) showed the effects of species specific tree growth reduction for VPD values above 1.5 kPa, decoupled from soil water limitations. This value can be used as an estimate at which the stomata of *Fagus sylvatica* (Lendzion und Leuschner 2008) and *Pseudotsuga menziesii* trees (Meinzer 1982) reduce conductance, which affects carbon uptake and therefore also carbon allocation and respiration by tree roots (Hsiao 1973). There was only one day in the two years, which represented a VPD > 1.5 kPa. This might be due to the type of calculation of VPD using the daily averaged. The VPD is therefore smoothed and represents only the average for the corresponding day, neglecting peaks. VPD values > 1 kPa were more present during 2023 (23 days) compared to 2024

(4 days). If VPD is calculated using the maximum T_a, values above 1.5 kPa were more common in 2023 (29 days) compared to 2024 (7 days) and the aforementioned hot moment is particularly affected by the high potential. Similar to daily averaged VPD > 0.75 kPa (or maximum VPD > 1 kPa) also leads to a negative relationship with R_s which is in contrast to the general captured pattern of positive relationship. The general comparison between available dates with Θ_S measurements and VPD revealed a negative correlation, indicating drier soil conditions with increasing VPD. Interestingly, we detected a higher average R_s in 2024 compared to 2023, but the two highest R_S rates were reached in 2023, correlating to the precipitation deficit within the ecosystem and reflected ecosystem stress within the soil. This might also be reasoned in the different precipitation patterns during both years, with larger gaps in 2023 (Supplemental Material Figure S2). Our results highlight the importance of high-resolution measurements to capture these specific hot moments, since an interpolation of R_s during these phases might lead to false conclusions.

Forest structural features and hot spots in the ECOSENSE Forest

In agreement with our hypotheses, we observed larger R_s for deciduous than for coniferous patches during summer (Figure 5). However, tree species did not affect soil respiration in winter, which is in contrast to Jochheim et al. (2022) and our hypothesis. However, a generally higher R_s for broadleaf species compared to coniferous species were also reported in the literature (Raich und Tufekciogul 2000). Longdoz et al. (2000) presented differences in R_s associated especially with *Fagus sylvatica* and *Pseudotsuga menziesii* patches in a slightly different climate. They underline differences in fresh leaf litter and lower C:N and lignin:N as indicators for decomposition as possible reasons for these patterns. Another reason might be the difference in transport processes through phloem, which was summarized by Kuzyakov und Gavrichkova (2010) to be lower for coniferous species compared to angiosperms, while the latter includes *Fagus sylvatica*. The differences in tree species also seem to reflect the spatial pattern in the ECOSENSE Forest, as abundance of *Fagus sylvatica* is higher in the northern part of the area. Especially during the summer season, we detected a larger variability compared to the winter season which could also be reasoned in the photosynthetic activity of trees within the forest. Regarding the strong heterogeneous and seasonal pattern, surprisingly, the deviation in R_s during autumn season from the average over the two-year measurement period was lowest, which would suggest that R_s during autumn could reflect the average R_s best. However, this might also be a specific effect of our research area.

We also point out to a slightly higher soil-gas diffusivity in the northern part (Table 2, Dystric Skeletic Cambisol). Differences between the soil types in regard to the other specified physical and chemical properties are not very pronounced except for a slightly higher soil-organic carbon content in the topsoil horizons, as well as the CEC and the phosphorous content. However, soil properties could be very heterogeneous throughout forest soils (Stutz und Lang 2023) and a clear border within the ECOSENSE Forest between the two existing soil types is yet to be determined. A transition zone could be located approximately in the center of the study area. Due to rather similar chemical and physical properties of the described soil profiles, we do not expect larger influences of soil properties on R_s. Biological analyses such as root distribution and microbial biomass, chemical and physical properties of each of the 35 plots within the ECOSENSE Forest, support our ideas that tree species and their associated micro-habitat (Hofmann et al. 2023; Köstler et al. 1968; Prescott und Grayston 2013; Spielvogel et al. 2016; Vesterdal 1999; Vesterdal et al. 2013) shape R_s.

For the plots influenced by deciduous trees we found up to a distance of 5 m a positive relationship with the average DBH only in summertime reflecting the phenology of trees. Similarly, Søe und Buchmann (2005) reported influences of DBH within a distance of 4 m. However, we can not confirm this pattern for all species composition as the negative effect associated with coniferous composition might be biased, as the relationship between the distance to the tree and the DBH is strongly positive for coniferous composition (averaging higher DBH further away from the stemfoot). The relation was also positive for mixed and deciduous composition but not as strong as for coniferous composition. Surprisingly, the tree height revealed negative relationship with R_s which is on the one hand again biased as trees in coniferous compositions were averaging higher compared to trees in deciduous composition. However, as trends within the compositions (deciduous, coniferous) were also negative, we also suggest a negative effect of tree height on R_s despite the bias between the composed groups. To our knowledge no effects of tree height have been stated

in the literature until now. This effect could partly be explained by a longer path for assimilates to reach the rhizosphere (Kuzyakov und Gavrichkova 2010).

Conclusion

The most novel result of our research was the predictive contribution of freely available grid-cell data from a large scale interpolated meteorological model. This model explained temporal patterns of soil respiration better than local measured parameters such as soil temperature or soil moisture. During special events such as the collapse in soil respiration during drought and partially the boost after rewetting were reflected by the meteorological model much better. One goal of soil respiration research is to predict the large-scale pattern of its contribution to the atmospheric CO_2 budget that could possibly be improved by using available grid interpolated weather data from national or international meteorological service. We suggest to test existing and current time series of soil respiration whether the high explanatory value of the averaged atmospheric vapour pressure prior to measurements, the vapour pressure deficit and the seasonality can improve the overall prediction quality. However, the small-scale local reflected the importance of non-meteorological parameters such as soil and vegetation. The contrast between deciduous and coniferous tree species had a significant contribution to explain the local variation of our data. With novel remote sensing techniques, high-resolution maps of tree-species distribution can be produced to scale up respiration models similar to the use of gridded meteorological data. However, our local soil respiration maps revealed places with very high or very low soil respiration independently from tree distribution. This could not yet be explained by the available parameters but were spatially consistent over two consecutive observation years. The next step will be a detailed soil analysis of the plot areas to identify the controls of these persistent spatial patterns.

Acknowledgements

We thank the laboratory team of the Chair of Soil Ecology for supporting the laboratory analysis. Furthermore, we want to thank Luna Reimer, Chris Huck and Fiona Bauer for their support during the start of the measurement campaign. We also thank the team members of the Chair of Sensor-based Geoinformatics and the Chair of Forest Growth and Dendroecology who worked on the forest tree inventory and helped in field, digitizing and validating the dataset. We thank Kristin Steger for the internal pre-submission review.

Statements and Declarations

Funding

Financial Support: This project was funded by the Deutsche Forschungsgemeinschaft (DFG) - Project-ID 459819582 – CRC-1537 ECOSENSE.

Competing Interests

The authors declare that they have no competing financial interest or personal relationships that could have appeared to influence the work reported in this paper.

Author Contributions

Julian Brzozon: Writing – original draft, Investigation, Methodology, Formal analysis. Patricia Schwarzkopf: Investigation. Friederike Lang: Writing – review & editing. Teja Kattenborn: Writing – review & editing, Investigation, Methodology, Formal analysis. Julian Frey: Writing – review & editing, Investigation, Methodology, Formal analysis. Helmer Schack-Kirchner: Writing – review & editing, Methodology, Conceptualization, Funding acquisition.

References

Barba J, Cueva A, Bahn M, Barron-Gafford GA, Bond-Lamberty B, Hanson PJ, Jaimes A, Kulmala L, Pumpanen J, Scott RL, Wohlfahrt G, Vargas R (2018) Comparing ecosystem and soil respiration: Review and key challenges of tower-based and soil measurements. Agricultural and Forest Meteorology 249:434–443. https://doi.org/10.1016/j.agrformet.2017.10.028

Bates D, Maechler M, Bolker B, Walker S (2015) Fitting Linear Mixed-Effects Models Using lme4:1–48. https://doi.org/10.18637/jss.v067.i01

Birch HF (1958) The effect of soil drying on humus decomposition and nitrogen availability. Plant and Soil 10:9–31. https://doi.org/10.1007/BF01343734

Bowling DR, McDowell NG, Bond BJ, Law BE, Ehleringer JR (2002) 13C content of ecosystem respiration is linked to precipitation and vapor pressure deficit. Oecologia 131:113–124. https://doi.org/10.1007/s00442-001-0851-y

Brunn M, Hafner BD, Zwetsloot MJ, Weikl F, Pritsch K, Hikino K, Ruehr NK, Sayer EJ, Bauerle TL (2022) Carbon allocation to root exudates is maintained in mature temperate tree species under drought. New Phytologist 235:965–977. https://doi.org/10.1111/nph.18157

Brunn M, Krüger J, Lang F (2023) Experimental drought increased the belowground sink strength towards higher topsoil organic carbon stocks in a temperate mature forest. Geoderma 431:116356. https://doi.org/10.1016/j.geoderma.2023.116356

Brunner I, Herzog C, Dawes MA, Arend M, Sperisen C (2015) How tree roots respond to drought. Front. Plant Sci. 6:547. https://doi.org/10.3389/fpls.2015.00547

Carey JC, Tang J, Templer PH et al (2016) Temperature response of soil respiration largely unaltered with experimental warming. Proceedings of the National Academy of Sciences of the United States of America 113:13797–13802. https://doi.org/10.1073/pnas.1605365113

Copernicus Climate Change Service (2019) ERA5-Land hourly data from 1950 to present. https://doi.org/10.24381/CDS.E2161BAC

Curiel Yuste J, Janssens IA, Carrara A, Ceulemans R (2004) Annual Q 10 of soil respiration reflects plant phenological patterns as well as temperature sensitivity. Global change biology 10:161–169. https://doi.org/10.1111/j.1529-8817.2003.00727.x

Darenova E, Adamič PC, Čater M (2024) Effect of temperature, water availability, and soil properties on soil CO2 efflux in beech-fir forests along the Carpathian Mts. CATENA 240:107974. https://doi.org/10.1016/j.catena.2024.107974

Davidson EA, Belk E, Boone RD (1998) Soil water content and temperature as independent or confounded factors controlling soil respiration in a temperate mixed hardwood forest. Global change biology 4:217–227. https://doi.org/10.1046/j.1365-2486.1998.00128.x

Davidson EA, Richardson AD, Savage KE, Hollinger DY (2006) A distinct seasonal pattern of the ratio of soil respiration to total ecosystem respiration in a spruce-dominated forest. Global change biology 12:230–239. https://doi.org/10.1111/j.1365-2486.2005.01062.x

DWD (2025) Index of /climate_environment/CDC/grids_germany/daily/hyras_de. https://opendata.dwd.de/climate_environment/CDC/grids_germany/daily/hyras_de/. Zugegriffen: 10. Juni 2025

Ekblad A, Högberg P (2001) Natural abundance of 13C in CO2 respired from forest soils reveals speed of link between tree photosynthesis and root respiration. Oecologia 127:305–308. https://doi.org/10.1007/s004420100667

Ekblad A, Boström B, Holm A, Comstedt D (2005) Forest soil respiration rate and delta13C is regulated by recent above ground weather conditions. Oecologia 143:136–142. https://doi.org/10.1007/s00442-004-1776-z

Epron D, Farque L, Lucot É, Badot P-M (1999) Soil CO2 efflux in a beech forest: dependence on soil temperature and soil water content. Ann. For. Sci. 56:221–226. https://doi.org/10.1051/forest:19990304

Fiedler J, Fuß R, Glatzel S, Hagemann U, Huth V, Jordan S, Jurasinski G, Kutzbach L, Maier M, Schäfer K, Weber T, Weymann D (2022) BEST PRACTICE GUIDELINE Measurement of carbon dioxide, methane and nitrous oxide fluxes between soil-vegetation-systems and the atmosphere using non-steady state chambers. Deutsche Bodenkundliche Gesellschaft (German Soil Science Society), Commission IV, Working Group Soil Gases, Task Force Standardisation

Frick C, Steiner H, Mazurkiewicz A, Riediger U, Rauthe M, Reich T, Gratzki A (2014) Central European high-resolution gridded daily data sets (HYRAS): Mean temperature and relative humidity. metz 23:15–32. https://doi.org/10.1127/0941-2948/2014/0560

Goulden ML, Munger JW, Fan S-M, Daube BC, Wofsy SC (1996) Exchange of Carbon Dioxide by a Deciduous Forest: Response to Interannual Climate Variability. Science 271:1576–1578. https://doi.org/10.1126/science.271.5255.1576

Grolemund G, Wickham H (2011) Dates and Times Made Easy with lubridate. J. Stat. Soft. 40:1–25. https://doi.org/10.18637/jss.v040.i03

Gutachterausschuss Forstliche Analytik (2022) Handbuch Forstliche Analytik: Eine Loseblatt-Sammlung der Analysemethoden im Forstbereich.; Bundesministerium für Verbraucherschutz, Ernährung und Landwirtschaft, Bonn.

Hansen J, Turkington R, Vogg G, Heim R, Beck E (1997) Conifer carbohydrate physiology: Updating classical views. Backhuys, Leiden

Hartge KH, Horn R (1989) Die physikalische Untersuchung von Böden. Enke, Stuttgart, Germany

Hayes AF, Cai L (2007) Using heteroskedasticity-consistent standard error estimators in OLS regression: an introduction and software implementation. Behavior research methods 39:709–722. https://doi.org/10.3758/bf03192961

Hereș A-M, Bragă C, Petritan AM, Petritan IC, Curiel Yuste J (2021) Spatial variability of soil respiration (R s) and its controls are subjected to strong seasonality in an even-aged European beech (Fagus sylvatica L.) stand. European J Soil Science 72:1988–2005. https://doi.org/10.1111/ejss.13116

Hofmann B, Dreyling L, Dal Grande F, Otte J, Schmitt I (2023) Habitat and tree species identity shape aboveground and belowground fungal communities in central European forests. Front. Microbiol. 14:1067906. https://doi.org/10.3389/fmicb.2023.1067906

Hsiao TC (1973) Plant Responses to Water Stress. Annu. Rev. Plant. Physiol. 24:519–570. https://doi.org/10.1146/annurev.pp.24.060173.002511

IPCC (2023) Climate Change 2022 – Impacts, Adaptation and Vulnerability: Working Group II Contribution to the Sixth Assessment Report of the Intergovernmental Panel on Climate Change. Cambridge University Press

IUSS (2022) World reference base for soil resources 2022: International soil classification system for naming soils and creating legends for soil maps / IUSS Working Group WRB. International Union of Soil Sciences, Vienna, Austria

Janssens IA, Pilegaard K (2003) Large seasonal changes in Q10 of soil respiration in a beech forest. Global change biology 9:911–918. https://doi.org/10.1046/j.1365-2486.2003.00636.x

Jochheim H, Wirth S, Gartiser V, Paulus S, Haas C, Gerke HH, Maier M (2022) Dynamics of Soil CO2 Efflux and Vertical CO2 Production in a European Beech and a Scots Pine Forest. Front. For. Glob. Change 5:826298. https://doi.org/10.3389/ffgc.2022.826298

Jovani-Sancho AJ, Cummins T, Byrne KA (2017) Collar insertion depth effects on soil respiration in afforested peatlands. Biol Fertil Soils 53:677–689. https://doi.org/10.1007/s00374-017-1210-4

Khomik M, Arain MA, McCaughey JH (2006) Temporal and spatial variability of soil respiration in a boreal mixedwood forest. Agricultural and Forest Meteorology 140:244–256. https://doi.org/10.1016/j.agrformet.2006.08.006

König N, Fortmann H (1996) Berichte des Forschungszentrum Waldökosysteme

Köstler JN, Brückner E, Bibelriether H (1968) Die Wurzeln der Waldbäume; Untersuchungen zur Morphologie der Waldbäume in Mitteleuropa. Verlag Paul Parey, Hamburg and Berlin., Germany

Kuzyakov Y (2006) Sources of CO2 efflux from soil and review of partitioning methods. Soil Biology and Biochemistry 38:425–448. https://doi.org/10.1016/j.soilbio.2005.08.020

Kuzyakov Y, Gavrichkova O (2010) REVIEW: Time lag between photosynthesis and carbon dioxide efflux from soil: a review of mechanisms and controls. Global change biology 16:3386–3406. https://doi.org/10.1111/j.1365-2486.2010.02179.x

Lejon DPH, Chaussod R, Ranger J, Ranjard L (2005) Microbial community structure and density under different tree species in an acid forest soil (Morvan, France). Microbial ecology 50:614–625. https://doi.org/10.1007/s00248-005-5130-8

Lendzion J, Leuschner C (2008) Growth of European beech (Fagus sylvatica L.) saplings is limited by elevated atmospheric vapour pressure deficits. Forest Ecology and Management 256:648–655. https://doi.org/10.1016/j.foreco.2008.05.008

Lenth RV (2023) emmeans: Estimated Marginal Means, aka Least-Squares Means.

Lloyd J, Taylor JA (1994) On the Temperature Dependence of Soil Respiration. Functional Ecology 8:315. https://doi.org/10.2307/2389824

Longdoz B, Yernaux M, Aubinet M (2000) Soil CO 2 efflux measurements in a mixed forest: impact of chamber disturbances, spatial variability and seasonal evolution. Global change biology 6:907–917. https://doi.org/10.1046/j.1365-2486.2000.00369.x

McAdam SAM, Brodribb TJ (2015) The evolution of mechanisms driving the stomatal response to vapor pressure deficit. Plant Physiol 167:833–843. https://doi.org/10.1104/pp.114.252940

McClain ME, Boyer EW, Dent CL, Gergel SE, Grimm NB, Groffman PM, Hart SC, Harvey JW, Johnston CA, Mayorga E, McDowell WH, Pinay G (2003) Biogeochemical Hot Spots and Hot Moments at the Interface

of Terrestrial and Aquatic Ecosystems. Ecosystems 6:301–312. https://doi.org/10.1007/s10021-003-0161-9

Meinzer FC (1982) The effect of vapor pressure on stomatal control of gas exchange in Douglas fir (Pseudotsuga menziesii) saplings. Oecologia 54:236–242. https://doi.org/10.1007/BF00378398

Moyano FE, Kutsch WL, Rebmann C (2008) Soil respiration fluxes in relation to photosynthetic activity in broad-leaf and needle-leaf forest stands. Agricultural and Forest Meteorology 148:135–143. https://doi.org/10.1016/j.agrformet.2007.09.006

Muñoz-Sabater J, Dutra E, Agustí-Panareda A, Albergel C, Arduini G, Balsamo G, Boussetta S, Choulga M, Harrigan S, Hersbach H, Martens B, Miralles DG, Piles M, Rodríguez-Fernández NJ, Zsoter E, Buontempo C, Thépaut J-N (2021) ERA5-Land: a state-of-the-art global reanalysis dataset for land applications. Earth Syst. Sci. Data 13:4349–4383. https://doi.org/10.5194/essd-13-4349-2021

Pebesma E (2018) Simple Features for R: Standardized Support for Spatial Vector Data. The R Journal 10:439. https://doi.org/10.32614/rj-2018-009

Pebesma EJ, Bivand R (2023) Spatial data science; With applications in R. CRC Press Taylor & Francis Group, Boca Raton

Prescott CE, Grayston SJ (2013) Tree species influence on microbial communities in litter and soil: Current knowledge and research needs. Forest Ecology and Management 309:19–27. https://doi.org/10.1016/j.foreco.2013.02.034

Qi Y, Xu M, Wu J (2002) Temperature sensitivity of soil respiration and its effects on ecosystem carbon budget: nonlinearity begets surprises. Ecological Modelling 153:131–142. https://doi.org/10.1016/S0304-3800(01)00506-3

R Core Team (2023) R: A Language and Environment for Statistical Computing. R Foundation for Statistical Computing, Vienna, Austria

Raich JW, Tufekciogul A (2000) Vegetation and soil respiration: Correlations and controls. Biogeochemistry 48:71–90. https://doi.org/10.1023/A:1006112000616

Rauthe M, Steiner H, Riediger U, Mazurkiewicz A, Gratzki A (2013) A Central European precipitation climatology – Part I: Generation and validation of a high-resolution gridded daily data set (HYRAS). metz 22:235–256. https://doi.org/10.1127/0941-2948/2013/0436

Razafimaharo C, Krähenmann S, Höpp S, Rauthe M, Deutschländer T (2020) New high-resolution gridded dataset of daily mean, minimum, and maximum temperature and relative humidity for Central Europe (HYRAS). Theor Appl Climatol 142:1531–1553. https://doi.org/10.1007/s00704-020-03388-w

Ruehr NK, Buchmann N (2010) Soil respiration fluxes in a temperate mixed forest: seasonality and temperature sensitivities differ among microbial and root-rhizosphere respiration. Tree physiology 30:165–176. https://doi.org/10.1093/treephys/tpp106

Ruehr NK, Knohl A, Buchmann N (2010) Environmental variables controlling soil respiration on diurnal, seasonal and annual time-scales in a mixed mountain forest in Switzerland. Biogeochemistry 98:153–170. https://doi.org/10.1007/s10533-009-9383-z

Sanginés de Cárcer P, Vitasse Y, Peñuelas J, Jassey VEJ, Buttler A, Signarbieux C (2018) Vapor-pressure deficit and extreme climatic variables limit tree growth. Global change biology 24:1108–1122. https://doi.org/10.1111/gcb.13973

Scapucci L, Krebs L, Burri S, Hörtnagl L, Buchmann N (2025) Soil and forest floor respiration already acclimated to increasing temperatures in a mixed deciduous forest. Ecological processes 14:71. https://doi.org/10.1186/s13717-025-00639-4

Schack-Kirchner H, Gaertig T, v. Wilpert K, Hildebrand EE (2001) A modified McIntyre and Phillip approach to measure top-soil gas diffusivity in-situ. Journal of Plant Nutrition and Soil Science 164:253–258. https://doi.org/10.1002/1522-2624(200106)164:3<253::AID-JPLN253>3.0.CO;2-G

Schindlbacher A, Rodler A, Kuffner M, Kitzler B, Sessitsch A, Zechmeister-Boltenstern S (2011) Experimental warming effects on the microbial community of a temperate mountain forest soil. Soil Biology and Biochemistry 43:1417–1425. https://doi.org/10.1016/j.soilbio.2011.03.005

Schindlbacher A, Wunderlich S, Borken W, Kitzler B, Zechmeister-Boltenstern S, Jandl R (2012) Soil respiration under climate change: prolonged summer drought offsets soil warming effects. Global change biology 18:2270–2279. https://doi.org/10.1111/j.1365-2486.2012.02696.x

Schwertmann U (1964) Differenzierung der Eisenoxide des Bodens durch Extraktion mit Ammoniumoxalat-Lösung. Journal of Plant Nutrition and Soil Science 105:194–202. https://doi.org/10.1002/jpln.3591050303

Scott-Denton L (2003) Spatial and temporal controls of soil respiration rate in a high-elevation, subalpine forest. Soil Biology and Biochemistry 35:525–534. https://doi.org/10.1016/S0038-0717(03)00007-5

Sims CA (1974) Seasonality in Regression. Journal of the American Statistical Association 69:618–626. https://doi.org/10.1080/01621459.1974.10480178

Snell HSK, Robinson D, Midwood AJ (2014) Minimising methodological biases to improve the accuracy of partitioning soil respiration using natural abundance 13C. Rapid Communications in Mass Spectrometry 28:2341–2351. https://doi.org/10.1002/rcm.7017

Søe ARB, Buchmann N (2005) Spatial and temporal variations in soil respiration in relation to stand structure and soil parameters in an unmanaged beech forest. Tree physiology 25:1427–1436. https://doi.org/10.1093/treephys/25.11.1427

Spielvogel S, Prietzel J, Kögel-Knabner I (2016) Stand scale variability of topsoil organic matter composition in a high-elevation Norway spruce forest ecosystem. Geoderma 267:112–122. https://doi.org/10.1016/j.geoderma.2015.12.001

Štursová M, Bárta J, Šantrůčková H, Baldrian P (2016) Small-scale spatial heterogeneity of ecosystem properties, microbial community composition and microbial activities in a temperate mountain forest soil. FEMS microbiology ecology 92. https://doi.org/10.1093/femsec/fiw185

Stutz KP, Lang F (2023) Forest ecosystems create pedogenic patchworks through woody debris, trees, and disturbance. Geoderma 429:116246. https://doi.org/10.1016/j.geoderma.2022.116246

Subke J-A, Reichstein M, Tenhunen JD (2003) Explaining temporal variation in soil CO2 efflux in a mature spruce forest in Southern Germany. Soil Biology and Biochemistry 35:1467–1483. https://doi.org/10.1016/S0038-0717(03)00241-4

Tamm O (1922) Om bestämning av de oorganiska komponenterna i markens gelkomplex

Tang J, Misson L, Gershenson A, Cheng W, Goldstein AH (2005a) Continuous measurements of soil respiration with and without roots in a ponderosa pine plantation in the Sierra Nevada Mountains. Agricultural and Forest Meteorology 132:212–227. https://doi.org/10.1016/j.agrformet.2005.07.011

Tang J, Baldocchi DD, Xu L (2005b) Tree photosynthesis modulates soil respiration on a diurnal time scale. Global change biology 11:1298–1304. https://doi.org/10.1111/j.1365-2486.2005.00978.x

Tarroso P, Velo-Anton G, Carvalho SB (2015) PHYLIN: an R package for phylogeographic interpolation. 15(2):349–357

Tarroso P, Carvalho SB, Velo-Antón G (2019) Phylin 2.0: Extending the phylogeographical interpolation method to include uncertainty and user-defined distance metrics. Molecular Ecology Resources 19:1081–1094. https://doi.org/10.1111/1755-0998.13010

Trüby P, Aldinger E (1989) Eine Methode zur Bestimmung austauschbarer Kationen in Waldböden. J Plant Nutrition & Soil 152:301–306. https://doi.org/10.1002/jpln.19891520307

Valentini R, Matteucci G, Dolman AJ, Schulze ED, Rebmann C, Moors EJ, Granier A, Gross P, Jensen NO, Pilegaard K, Lindroth A, Grelle A, Bernhofer C, Grünwald T, Aubinet M, Ceulemans R, Kowalski AS, Vesala T, Rannik U, Berbigier P, Loustau D, Gudmundsson J, Thorgeirsson H, Ibrom A, Morgenstern K, Clement R (2000) Respiration as the main determinant of carbon balance in European forests. Nature 404:861–865. https://doi.org/10.1038/35009084

Vesterdal L (1999) Influence of soil type on mass loss and nutrient release from decomposing foliage litter of beech and Norway spruce. Can. J. For. Res. 29:95–105. https://doi.org/10.1139/x98-182

Vesterdal L, Elberling B, Christiansen JR, Callesen I, Schmidt IK (2012) Soil respiration and rates of soil carbon turnover differ among six common European tree species. Forest Ecology and Management 264:185–196. https://doi.org/10.1016/j.foreco.2011.10.009

Vesterdal L, Clarke N, Sigurdsson BD, Gundersen P (2013) Do tree species influence soil carbon stocks in temperate and boreal forests? Forest Ecology and Management 309:4–18. https://doi.org/10.1016/j.foreco.2013.01.017

Wang Y, Hao Y, Cui XY, Zhao H, Xu C, Zhou X, Xu Z (2014a) Responses of soil respiration and its components to drought stress. J Soils Sediments 14:99–109. https://doi.org/10.1007/s11368-013-0799-7

Wang X, Liu L, Piao S, Janssens IA, Tang J, Liu W, Chi Y, Wang J, Xu S (2014b) Soil respiration under climate warming: differential response of heterotrophic and autotrophic respiration. Global change biology 20:3229–3237. https://doi.org/10.1111/gcb.12620

Werner C, Wallrabe U, Christen A, Comella L, Dormann C, Göritz A, Grote R, Haberstroh S, Jouda M, Kiese R, Koch B, Korvink J, Kreuzwieser J, Lang F, Müller J, Prucker O, Reiterer A, Rühe J, Rupitsch S, Schack-Kirchner H, Schmitt K, Stobbe N, Weiler M, Woias P, Wöllenstein J (2024) ECOSENSE - Multi-scale

quantification and modelling of spatio-temporal dynamics of ecosystem processes by smart autonomous sensor networks. RIO 10. https://doi.org/10.3897/rio.10.e129357

Wickham H (2016) Data Analysis. ggplot2:189–201. https://doi.org/10.1007/978-3-319-24277-4_9

Wickham H, Averick M, Bryan J, Chang W, McGowan L, François R, Grolemund G, Hayes A, Henry L, Hester J, Kuhn M, Pedersen T, Miller E, Bache S, Müller K, Ooms J, Robinson D, Seidel D, Spinu V, Takahashi K, Vaughan D, Wilke C, Woo K, Yutani H (2019) Welcome to the Tidyverse. JOSS 4:1686. https://doi.org/10.21105/joss.01686